Proceedings of ASME 2014 Dynamic Systems and Control Conference
DSCC 2014
October 22-24, 2014, San Antonio, Texas, USA

DSCC2014-6358

STABILITY ANALYSIS OF NONLINEAR CONNECTED VEHICLE SYSTEMS

Linjun Zhang*
Department of Mechanical Engineering
University of Michigan
Ann Arbor, Michigan 48109
Email: linjunzh@umich.edu

Gábor Orosz
Department of Mechanical Engineering
University of Michigan
Ann Arbor, Michigan 48109
Email: orosz@umich.edu

ABSTRACT

In this paper, we investigate the nonlinear dynamics of connected vehicle systems. Vehicle-to-vehicle (V2V) communication is exploited when controlling the longitudinal motion of a few vehicles in the traffic flow. In order to achieve the desired system-level behavior, the plant stability and the head-to-tail string stability are characterized at the nonlinear level using Lyapunov functions. A motif-based approach is utilized that allows modular design for large-scale vehicle networks. Stability analysis of motifs are summarized using stability diagrams, which are validated by numerical simulations.

1 INTRODUCTION

Wireless vehicle-to-vehicle (V2V) communication technologies can be utilized to monitor distant vehicles beyond the line-of-sight in vehicular traffic. The traditional way of utilizing V2V communication is to start with a designated leading vehicle and then add following vehicles that monitor the motion of the vehicle immediately ahead by radar and also communicate with the leader. This setup is often referred to as cooperative adaptive cruise control (CACC) [1,2]. Creating such systems may be possible for a few vehicles, but such design is not scalable for large systems due to the limited range of the wireless communication and the cost of sensors required for every vehicle. Moreover, long tightly-controlled platoons may severely limit modularity of the entire transportation system.

To solve this issue, the concept of connected cruise control (CCC) was proposed [3–6], which relies on the ad-hoc wireless V2V communication and does not require a designated leader. CCC can be used to assist human drivers or to automatically regulate the longitudinal motion of vehicles. CCC also allows one to incorporate in a platoon with vehicles that are not equipped with radar and/or communication devices. When CCC vehicles are mixed into the flow of non-CCC vehicles, a connected vehicle system (CVS) arises. By appropriately designing the connectivity structure and the control gains, it is possible to ensure smooth flow when stop-and-go oscillations develop for a chain of human-driven vehicles. However, allowing more flexibility in the network architecture increases the complexity of analysis and design of large-scale CVS. To handle this problem, a motif-based approach was proposed in [3, 7] that is based on the idea that connected vehicle networks can be constructed using network motifs: simple networks where a CCC vehicle at the tail monitors the motion of its immediate predecessor and the motion of a distant vehicle; see already Fig. 2. By analyzing the dynamics of individual motifs and characterizing the effects of interactions between motifs may allow one to modularly design CVS that are scalable and robust against the variations in the connectivity structure.

Plant stability and string stability can be used to evaluate the performance of vehicle platoons. Plant stability means that, if the head vehicle moves at a constant speed, all following vehicles approach that speed. String stability characterizes the ability of a platoon in attenuating velocity perturbations arising from vehicles ahead. In this paper, we compare the velocity perturbation of the head vehicle and the tail vehicle, and thus evaluate the head-to-tail string stability. Plant stability and the string stability of motifs were analyzed in [3, 7] based on linearized models, but

*Address all correspondence to this author.

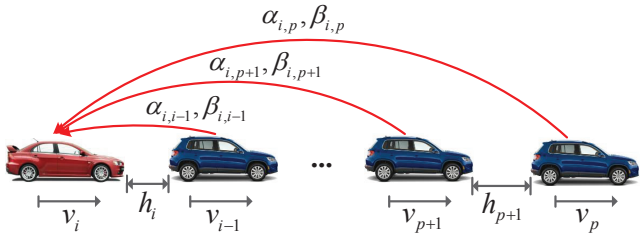

FIGURE 1. Communication network where a CCC vehicle (at the tail) utilizes the information received from multiple vehicles ahead. The headway and velocity of vehicle j are denoted by h_j and v_j, respectively, where $j = p, \dots, i$. $\alpha_{i,j}$ and $\beta_{i,j}$ are control gains corresponding to the link between vehicle i and vehicle j.

such analysis is limited to the close vicinity of the equilibrium. It was shown in [8] that due to nonlinearities, small perturbations may decay while large perturbations may be amplified for certain parameter combinations. In this paper, we directly investigate the nonlinear dynamics of motifs and hence overcome the limitations caused by linearized models. The Lyapunov approach is applied to seek conditions for plant stability and for head-to-tail string stability at the nonlinear level. Stability conditions for simple motifs are summarized using stability diagrams in the plane of control gains.

2 DYNAMICS AND STABILITY OF CONNECTED VEHICLE SYSTEMS

In this section, we present dynamic car-following models for CCC vehicles and for network motifs that consist of a chain of non-CCC vehicles and a CCC vehicle at the tail. The mathematical definition of plant stability and head-to-tail string stability are also given to evaluate the performance of vehicle networks.

2.1 Dynamics of Connected Cruise Control

In Fig. 1, the CCC vehicle i (at the tail) monitors the motion of vehicles $j = p, \dots, i-1$ by using V2V communication. Here h_j denotes the distance between vehicle $j-1$ and vehicle j, called "headway", and v_j represents the velocity of vehicle j. We assume that the V2V communication provides information about positions and velocities of other vehicles so that the corresponding headways and relative velocities can be calculated. For simplicity, the delays for receiving information are neglected in this paper. Then, based on [3], the CCC vehicle can be modelled by

$$\begin{aligned} \dot{h}_i &= v_{i-1} - v_i \,, \\ \dot{v}_i &= \sum_{j=p}^{i-1} \alpha_{i,j} \left(V_i\left(\frac{1}{i-j} \sum_{k=j+1}^{i} h_k \right) - v_i \right) + \sum_{j=p}^{i-1} \beta_{i,j} \left(v_j - v_i \right) , \end{aligned} \tag{1}$$

where $\alpha_{i,j}$ and $\beta_{i,j}$ are control gains for headways and relative velocities, respectively. Note that $i > j$ since we assume that V2V information is only utilized upstream. When there is no connection between vehicle j and vehicle i, we have $\alpha_{i,j} = \beta_{i,j} = 0$. Thus, model (1) can be also used for non-CCC vehicles by setting $\alpha_{i,j} = \beta_{i,j} = 0$ for all $j < i-1$.

The range policy $V_i(h)$ gives the desired velocity for vehicle i, and the quantity $\frac{1}{i-j}\sum_{k=j+1}^{i} h_k$ represents the average headway between vehicle i and vehicle j, allowing one to compare desired velocities obtained for different j's. We assume that all vehicles use the same range policy function, i.e., $V_i(h) = V(h)$ for all i. And we use the range policy function

$$V(h) = \begin{cases} 0 \,, & \text{if} \quad h \le h_{\rm st} \,, \\ \frac{v_{\max}}{2} \left[1 - \cos\left(\pi \frac{h - h_{\rm st}}{h_{\rm go} - h_{\rm st}} \right) \right] , & \text{if} \quad h_{\rm st} < h < h_{\rm go} \,, \\ v_{\max} \,, & \text{if} \quad h \ge h_{\rm go} \,. \end{cases} \tag{2}$$

The physical meaning of (2) is as follows. When the headway is below a threshold $h \le h_{\rm st}$, the vehicle tends to stop for safety reasons. For large headways $h \ge h_{\rm go}$, the vehicle aims to maintain the preset maximum velocity $v_{\max}$. Between $h_{\rm st}$ and $h_{\rm go}$, the desired velocity monotonically increases with the headway. In this paper, we use the following parameter values

$$h_{\rm st} = 5 \ [\rm m] \quad h_{\rm go} = 35 \ [\rm m] \,, \quad v_{\max} = 30 \ [\rm m/s] \,, \tag{3}$$

which corresponds to the data collected in real traffic [8].

Considering a platoon of $n+1$ vehicles where all vehicles use that same range policy, model (1) ensures the the existence of uniform flow equilibrium

$$h_i(t) \equiv h^* \,, \quad v_i(t) \equiv v^* = V(h^*) \,, \quad i = 0, \dots, n \,, \tag{4}$$

which is independent of platoon length, connectivity structures, and control gains.

2.2 Motifs for Connected Vehicle Systems

To decrease the complexity of stability analysis for connected vehicle networks, a motif-based approach was proposed in [3, 7]. The key idea is that vehicle networks can be constructed from network motifs and analyzing these motifs allows one to modularly design CVS so that the design remains scalable for large systems. Motif n is depicted in Fig. 2(a), where the CCC vehicle n at the tail utilizes data about the motion of vehicle $n-1$ and vehicle 0, while the other vehicles $j = 1, \dots, n-1$ only react to the motion of the vehicle immediately ahead.

For simplicity, we assume that the control gains are non-negative and also are identical for links of same length, i.e.,

$\alpha_{i,j}=\alpha_{i-j}\geq 0$ and $\beta_{i,j}=\beta_{i-j}\geq 0$. Applying (1), the governing equations for motif n become

$$\begin{aligned}
&\dot{h}_j = v_{j-1}-v_j\,,\\
&\dot{v}_j = \alpha_1\big(V(h_j)-v_j\big)+\beta_1(v_{j-1}-v_j)\,,\\
&\dot{h}_n = v_{n-1}-v_n\,,\\
&\dot{v}_n = \alpha_1\big(V(h_n)-v_n\big)+\beta_1(v_{n-1}-v_n)\\
&\quad+\alpha_n\left(V\left(\frac{1}{n}\sum_{k=1}^{n}h_k\right)-v_n\right)+\beta_n(v_0-v_n)\,,
\end{aligned}\tag{5}$$

for $j=1,\dots,n-1$.

Define the perturbations about the uniform flow equilibrium (4) such that

$$\tilde{h}_i = h_i-h^*\,,\quad \tilde{v}_i = v_i-v^*=v_i-V(h^*)\,,\quad i=0,\dots,n\,.\tag{6}$$

Substituting (6) into (5) results in

$$\begin{aligned}
&\dot{\tilde{h}}_j = \tilde{v}_{j-1}-\tilde{v}_j\,,\\
&\dot{\tilde{v}}_j = \alpha_1\big(V(\tilde{h}_j+h^*)-V(h^*)-\tilde{v}_j\big)+\beta_1(\tilde{v}_{j-1}-\tilde{v}_j)\,,\\
&\dot{\tilde{h}}_n = \tilde{v}_{n-1}-\tilde{v}_n\,,\\
&\dot{\tilde{v}}_n = \alpha_1\big(V(\tilde{h}_n+h^*)-V(h^*)-\tilde{v}_n\big)+\beta_1(\tilde{v}_{n-1}-\tilde{v}_n)\\
&\quad+\alpha_n\left(V\left(\frac{1}{n}\sum_{k=1}^{n}\tilde{h}_k+h^*\right)-V(h^*)-\tilde{v}_n\right)+\beta_n(\tilde{v}_0-\tilde{v}_n)\,,
\end{aligned}\tag{7}$$

for $j=1,\dots,n-1$.

Generally, the headway can be any positive value, i.e., $h_i\in\mathbb{R}_+$ for $i=1,\dots,n$, but the domain of our interest is the normal operating domain $\mathscr{D}=\{h_{\rm st}<h_i<h_{\rm go}\}$ that covers the whole velocity domain $0<v<v_{\max}$; cf. (2). It follows that the equilibrium headway $h^*\in\mathscr{D}$. Then, based on the mean value theorem, there exist variables $\xi_j,\eta_n\in\mathscr{D}$ such that

$$\begin{aligned}
V(\tilde{h}_j+h^*)-V(h^*)&=V'(\xi_j)\tilde{h}_j\,,\\
V\left(\frac{1}{n}\sum_{k=1}^{n}\tilde{h}_k+h^*\right)-V(h^*)&=V'(\eta_n)\frac{1}{n}\sum_{k=1}^{n}\tilde{h}_k\,,
\end{aligned}\tag{8}$$

where the prime denotes differentiation with respect to h, and $\xi_j,\ \eta_n\in\mathscr{D}$ depend on headway perturbations such that

$$\begin{aligned}
\xi_j &= h_{\rm st}+\frac{h_{\rm go}-h_{\rm st}}{\pi}K(\tilde{h}_j)\,,\\
\eta_n &= h_{\rm st}+\frac{h_{\rm go}-h_{\rm st}}{\pi}K\left(\sum_{k=1}^{n}\tilde{h}_k\right)\,,
\end{aligned}\tag{9}$$

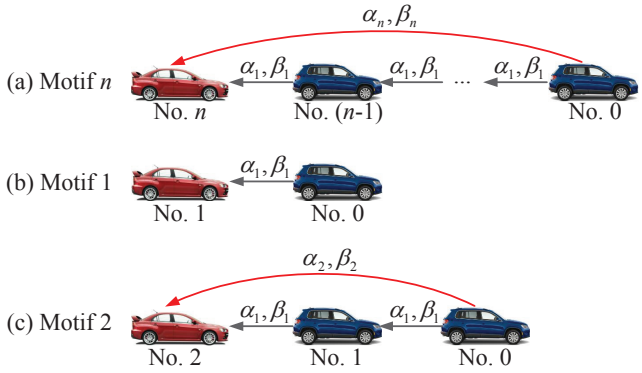

FIGURE 2. Network motifs with the CCC vehicle at the tail. Control gains are shown along the links.

where

$$K(\tilde{h})=\begin{cases}J(\tilde{h})\,, & \text{if }\ \tilde{h}\in\left(h_{\rm st}-h^*,\ \frac{h_{\rm st}+h_{\rm go}-2h^*}{2}\right]\,,\\ \pi-J(\tilde{h})\,, & \text{if }\ \tilde{h}\in\left(\frac{h_{\rm st}+h_{\rm go}-2h^*}{2},\ h_{\rm go}-h^*\right)\,,\end{cases}\tag{10}$$

where

$$J(\tilde{h})=\arcsin\left(\frac{2(h_{\rm go}-h_{\rm st})\big(V(\tilde{h}+h^*)-V(h^*)\big)}{\pi v_{\max}\tilde{h}}\right)\,,\tag{11}$$

which can be obtained from (2). According to (3), we also have

$$V'(\xi_j)\,,V'(\eta_n)\in\big(0,\pi/2\big]\,,\quad\forall\xi_j,\eta_n\in\mathscr{D}\,.\tag{12}$$

Substituting (8) into (7) yields

$$\begin{aligned}
&\dot{\tilde{h}}_j = \tilde{v}_{j-1}-\tilde{v}_j\,,\\
&\dot{\tilde{v}}_j = \varphi_1(\xi_j)\tilde{h}_j-\kappa_1\tilde{v}_j+\beta_1\tilde{v}_{j-1}\,,\\
&\dot{\tilde{h}}_n = \tilde{v}_{n-1}-\tilde{v}_n\,,\\
&\dot{\tilde{v}}_n = \varphi_1(\xi_n)\tilde{h}_n+\varphi_n(\eta_n)\sum_{k=1}^{n}\tilde{h}_k-(\kappa_1+\kappa_n)\tilde{v}_n+\beta_1\tilde{v}_{n-1}+\beta_n\tilde{v}_0\,,
\end{aligned}\tag{13}$$

for $j=1,\dots,n-1$, where

$$\varphi_m(h)=\frac{\alpha_m V'(h)}{m}\,,\quad \kappa_m=\alpha_m+\beta_m\,,\tag{14}$$

for $m=1,\dots,n$. System (13) can be written in the form

$$\begin{aligned}
\dot{X}_n &= A_n(\Xi_n)X_n+B_n\tilde{v}_0\,,\\
y &= \tilde{v}_n = C_nX_n\,,
\end{aligned}\tag{15}$$

where $\Xi_n = [\xi_1, \ldots, \xi_n, \eta_n]^{\mathrm{T}} \in \mathscr{D}^{n+1}$ and

$$\begin{aligned} &X_n = \left[x_1^{\mathrm{T}} \cdots x_n^{\mathrm{T}} \right]^{\mathrm{T}}, \quad A_n(\Xi_n) = I_n \otimes D + G_n \otimes E + H, \\ &B_n = \left[1\ \beta_1\ 0 \cdots 0\ \beta_n \right]^{\mathrm{T}}, \quad C_n = \left[0 \cdots 0\ 1 \right]. \end{aligned} \tag{16}$$

Here $\otimes$ denotes the Kronecker product, I_n is an n-dimensional identity matrix, and other matrices are given by

$$\begin{aligned} &x_i = \begin{bmatrix} \tilde{h}_i \\ \tilde{v}_i \end{bmatrix}, \quad D = \begin{bmatrix} 0 & -1 \\ \varphi_1(\xi_j) & -\kappa_1 \end{bmatrix}, \quad E = \begin{bmatrix} 0 & 1 \\ 0 & \beta_1 \end{bmatrix}, \\ &G_n = [g_{ij}]_{n\times n}, \quad g_{ij} = \begin{cases} 1, & \text{if } i = j+1, \\ 0, & \text{otherwise}, \end{cases} \\ &H = [h_{ij}]_{2n\times 2n}, \quad h_{ij} = \begin{cases} \varphi_n(\eta_n), & \text{if } i = n \text{ and } j = 2k+1, \\ -\kappa_n, & \text{if } i = j = 2n, \\ 0, & \text{otherwise}, \end{cases} \end{aligned} \tag{17}$$

for $k = 0, \ldots, n-1$. Notice that $A_n(\Xi_n)$ depends on the states $\tilde{h}_1, \ldots, \tilde{h}_n$ (see (9)). We emphasize that (15) is equivalent to the original nonlinear model (7) since no approximation is used through the derivation.

2.3 Stability of Connected Vehicle Systems

Plant stability and head-to-tail string stability are used to evaluate the performance of connected vehicle systems. Plant stability means that, when the head vehicle moves with a constant speed, perturbations in the states of following vehicles decay to zero [9]. That is, $\tilde{v}_0 \equiv 0$ in (7) or (15) leads to

$$\tilde{h}_i, \tilde{v}_i \to 0, \quad \text{as } t \to \infty, \quad i = 1, \ldots, n. \tag{18}$$

Head-to-tail string stability requires that the disturbances arising in the velocity of head vehicle are attenuated by the tail vehicle [3]. There are a variety of ways to characterize the head-to-tail string stability depending on the disturbance signals and the norm used. In this paper, the platoon is said to be head-to-tail string stable if, for an arbitrary sinusoidal perturbation arising in the velocity of the head vehicle, the magnitude of the steady-state perturbation in the velocity of the tail vehicle is smaller than that of the head vehicle. That is, suppose that $\tilde{v}_0(t) = a\sin(\omega t + \phi)$, where $a, \phi \in \mathbb{R}$ and $\omega \in \mathbb{R}_+$ are all constants, then the platoon is head-to-tail string stable if

$$\|\tilde{v}_{n\mathrm{s}}\|_\infty < \|\tilde{v}_0\|_\infty, \tag{19}$$

where the subscript "s" denotes steady-state response after transients and the infinite-norm $\|\tilde{v}_{j\mathrm{s}}\|_\infty = \sup_{t>0} |\tilde{v}_{j\mathrm{s}}(t)|$ gives the peak value of $|\tilde{v}_{j\mathrm{s}}(t)|$. Note that head-to-tail string stability allows that disturbances generated by the head vehicle 0 may be amplified by some vehicles in the platoon but finally attenuated when reaching the tail vehicle n. This definition also allows one to compare the dynamics of platoons of the same length but different connectivity structures.

At the linear level, plant stability and head-to-tail string stability can be investigated by using the transfer function $G_{n,0}(s) = \tilde{V}_n(s)/\tilde{V}_0(s)$, where $\tilde{V}_i(s)$ denotes the Laplace transformation of $\tilde{v}_i(t)$. The plant stability (18) is equivalent to that all poles of $G_{n,0}(s)$ are in the left-half complex plane. On the other hand, the head-to-tail string stability (19) is guaranteed if the magnitude of transfer function is smaller than 1 for all positive frequencies, i.e., $|G_{n,0}(\mathrm{j}\omega)| < 1$ for $\forall \omega \in \mathbb{R}_+$, where $\mathrm{j}^2 = -1$. However, the linear stability results may not be used to characterize the behavior of the nonlinear system. To handle this problem, we directly analyze the nonlinear dynamics of vehicle networks using Lyapunov techniques. For the sake of simplicity, we focus on the stability analysis of simple motifs at the nonlinear level.

3 STABILITY ANALYSIS OF MOTIF 1

In this section, we study the nonlinear dynamics of motif 1 (see Fig. 2(b)), which represents a simple predecessor following configuration where the following vehicle only reacts to the motion of the vehicle immediately ahead. Based on (5), the governing equations for motif 1 are given by

$$\begin{aligned} &\dot{h}_1 = v_0 - v_1, \\ &\dot{v}_1 = \alpha_1 \big(V(h_1) - v_1 \big) + \beta_1 (v_0 - v_1). \end{aligned} \tag{20}$$

Substituting (6) into (20) yields the perturbation model

$$\begin{aligned} &\dot{\tilde{h}}_1 = \tilde{v}_0 - \tilde{v}_1, \\ &\dot{\tilde{v}}_1 = \alpha_1 \big(V(\tilde{h}_1 + h^*) - V(h^*) - \tilde{v}_1 \big) + \beta_1 (\tilde{v}_0 - \tilde{v}_1), \end{aligned} \tag{21}$$

which can be written in the following form

$$\begin{aligned} &\dot{x}_1 = A_1(\xi_1) x_1 + B_1 \tilde{v}_0, \\ &\tilde{v}_1 = C_1 x_1, \end{aligned} \tag{22}$$

where

$$\begin{aligned} &x_1 = \begin{bmatrix} \tilde{h}_1 \\ \tilde{v}_1 \end{bmatrix}, \quad A_1(\xi_1) = \begin{bmatrix} 0 & -1 \\ \varphi_1(\xi_1) & -\kappa_1 \end{bmatrix}, \\ &B_1 = \begin{bmatrix} 1 \\ \beta_1 \end{bmatrix}, \qquad C_1 = \begin{bmatrix} 0\ 1 \end{bmatrix}, \end{aligned} \tag{23}$$

cf. (15)–(17). The form of the models (20), (21), and (22) correspond to the general forms (5), (7) and (15), respectively.

3.1 Plant Stability of Motif 1

When analyzing the plant stability, we neglect the perturbations in the velocity of the head vehicle, i.e., $\tilde{v}_0(t) \equiv 0$ in (22). Then, based on the Lyapunov theory [10], the system is plant stable if there exists a Lyapunov function

$$L = x_1^{\mathrm{T}} P x_1 > 0\,, \quad \dot{L} = x_1^{\mathrm{T}} \big((A_1(\xi_1))^{\mathrm{T}} P + P A_1(\xi_1) \big) x_1 < 0\,. \tag{24}$$

Here P is a positive definite matrix. That is

$$P = \begin{bmatrix} p_1 & p_2 \\ p_2 & p_3 \end{bmatrix}, \quad p_1 > 0\,, \quad p_3 > 0\,, \quad p_1 p_3 - p_2^2 > 0\,. \tag{25}$$

To ensure $\dot{L} < 0$ in (24), the matrix $(A_1(\xi_1))^{\mathrm{T}} P + P A_1(\xi_1)$ has to be negative definite for $\forall \xi_1 \in \mathscr{D}$. This is equivalent to that the coefficients of the characteristic polynomial

$$\det\big(\lambda I_2 - \big((A_1(\xi_1))^{\mathrm{T}} P + P A_1(\xi_1)\big)\big) = \lambda^2 + \gamma_1 \lambda + \gamma_0\,, \tag{26}$$

are positive for $\forall \xi_1 \in \mathscr{D}$, that is,

$$\begin{aligned} &\gamma_1 = 2\big(1 - \varphi_1(\xi_1)\big) p_2 + 2\kappa_1 p_3 > 0\,, \\ &\gamma_0 = -p_3^2 \big(\varphi_1(\xi_1)\big)^2 + 2\big(p_1 p_3 - 2p_2^2 - \kappa_1 p_2 p_3\big)\varphi_1(\xi_1) \\ &\quad - (p_1 + \kappa_1 p_2)^2 > 0\,. \end{aligned} \tag{27}$$

The equivalence above is because $(A_1(\xi_1))^{\mathrm{T}} P + P A_1(\xi_1)$ is symmetric, and thus there exists an orthonormal matrix $Z(\xi_1)$ such that $(A_1(\xi_1))^{\mathrm{T}} P + P A_1(\xi_1) = Z^{\mathrm{T}}(\xi_1) \Delta(\xi_1) Z(\xi_1)$ where $\Delta(\xi_1)$ is a diagonal matrix. Substituting this in (24), we have $\dot{L} = \big(Z(\xi_1) x_1\big)^{\mathrm{T}} \Delta(\xi_1) \big(Z(\xi_1) x_1\big)$. As a result, $\dot{L}$ is negative definite if $\Delta(\xi_1)$ is Hurwitz for $\forall \xi_1 \in \mathscr{D}$.

For positive control gains, we have $\varphi_1(\xi_1) > 0$; cf. (14). Thus, to ensure $\gamma_0 > 0$ for $\forall \xi_1 \in \mathscr{D}$, we must have $(p_1 + \kappa_1 p_2) = 0$. Considering this together with (14) and (25), we get

$$p_1 = -\kappa_1 p_2 > 0\,, \quad p_2 < 0\,, \quad \kappa_1 p_3 > -p_2\,. \tag{28}$$

Plugging (14) and the first equation of (28) into (27) yields

$$\begin{aligned} \big(p_3 - V'(\xi_1) p_2\big)\alpha_1 + p_2 + p_3 \beta_1 > 0\,, \\ \big(-V'(\xi_1) p_3^2 - 4p_2 p_3\big)\alpha_1 - 4p_2^2 - 4p_2 p_3 \beta_1 > 0\,. \end{aligned} \tag{29}$$

To ensure these inequalities, the minima of the left hand sides must be positive. Considering (12), we obtain

$$\begin{aligned} p_3 \alpha_1 + p_2 + p_3 \beta_1 > 0\,, \\ \left(-\frac{\pi p_3^2}{2} - 4p_2 p_3 \right)\alpha_1 - 4p_2^2 - 4p_2 p_3 \beta_1 > 0\,, \end{aligned} \tag{30}$$

which results in

$$\alpha_1 + \beta_1 + \frac{p_2}{p_3} > 0\,, \quad \left(\frac{\pi p_3}{8 p_2} + 1 \right)\alpha_1 + \beta_1 + \frac{p_2}{p_3} > 0\,. \tag{31}$$

Choosing p_1, p_2, p_3 according to (28) and using control gains α_1, β_1 given by (31), one can guarantee (27). Hence condition (24) is satisfied, which implies that $x_1 \to 0$ in (22) as $t \to \infty$, i.e., $\tilde{h}_1 \to 0$ and $\tilde{v}_1 \to 0$.

Observing the stable domain given by (31) in the (α_1, β_1)-plane for different values of p_2/p_3, we obtain a sufficiently large stable domain when $p_2/p_3 = -\pi/8$. In particular, we choose $p_2 = -\pi$ and $p_3 = 8$ and draw the corresponding plant stable domain in Section 5.

3.2 String Stability of Motif 1

As mentioned in Section 2, when evaluating the string stability of motif 1, we assume that the perturbation in the velocity of the head vehicle is a sinusoidal signal such that

$$\tilde{v}_0(t) = r_0 \cos(\omega t) + s_0 \sin(\omega t) = a \sin(\omega t + \phi)\,, \tag{32}$$

where $r_0, s_0 \in \mathbb{R}$, $\omega \in \mathbb{R}_+$ are constants while $a = \sqrt{r_0^2 + s_0^2}$ and $\phi = \arctan(r_0/s_0)$ denote the amplitude and phase, respectively. It follows that

$$\|\tilde{v}_0\|_\infty = \sup_{t \geq 0} |\tilde{v}_0(t)| = \sqrt{r_0^2 + s_0^2}\,. \tag{33}$$

Note that $\tilde{v}_0(t+T) = \tilde{v}_0(t)$ where the period is $T = 2\pi/\omega$. Here we show that, when the sufficient condition for plant stability (24) is ensured, the steady-state perturbations of vehicle 1 are also T-periodic. Considering $t = t + T$ in (21) and subtracting (21) from the result, we obtain

$$\begin{aligned} &\dot{\tilde{h}}_1(t+T) - \dot{\tilde{h}}_1(t) = -\big(\tilde{v}_1(t+T) - \tilde{v}_1(t)\big)\,, \\ &\dot{\tilde{v}}_1(t+T) - \dot{\tilde{v}}_1(t) = \alpha_1 \big(V(\tilde{h}_1(t+T) + h^*) - V(\tilde{h}_1(t) + h^*)\big) \\ &\qquad - \kappa_1 \big(\tilde{v}_1(t+T) - \tilde{v}_1(t)\big)\,. \end{aligned} \tag{34}$$

When vehicles travel in the normal operating domain, i.e., $\tilde{h}_1(t) + h^* \in \mathscr{D}$, we can utilize the mean value theorem and state that there exists a variable $\psi \in \mathscr{D}$ satisfying

$$V\big(\tilde{h}_1(t+T) + h^*\big) - V\big(\tilde{h}_1(t) + h^*\big) = V'(\psi)\big(\tilde{h}_1(t+T) - \tilde{h}_1(t)\big)\,, \tag{35}$$

cf. (8)–(11). Substituting (35) into (34), we can write the result in the form

$$\dot{e}(t) = A_1(\psi)e(t)\,, \tag{36}$$

where

$$e(t) = x_1(t+T) - x_1(t)\,, \quad A_1(\psi) = \begin{bmatrix} 0 & -1 \\ \varphi_1(\psi) & -\kappa_1 \end{bmatrix}, \tag{37}$$

and x_1 is defined in (17). Note that $A_1(\psi)$ in (37) is equivalent to $A_1(\xi_1)$ in (23) in terms of bounds for their elements. As result, if the plant stability condition (31) is satisfied, one can use the same matrix P as in (24) to define the Lyapunov function such that, for $\forall \psi \in \mathscr{D}$, the following condition holds

$$L = e^{\mathrm{T}}Pe > 0\,, \quad \dot{L} = e^{\mathrm{T}}\big((A_1(\psi))^{\mathrm{T}}P + PA_1(\psi)\big)e < 0\,. \tag{38}$$

This implies that $e(t) \to 0$ as $t \to \infty$. That is, the steady-state error is $e_{\mathrm{s}}(t) = 0$ yielding $x_{1\mathrm{s}}(t+T) = x_{1\mathrm{s}}(t)$.

Since $x_{1\mathrm{s}}(t)$ is T-periodic, it can be represented by the Fourier series such that

$$x_{1\mathrm{s}}(t) = \sum_{k=1}^{\infty} r_{1,k}\cos(k\omega t) + s_{1,k}\sin(k\omega t)\,, \tag{39}$$

where $r_{1,k}, s_{1,k} \in \mathbb{R}^2$ are constant vectors. Applying trigonometric identities, one may obtain

$$x_{1\mathrm{s}}(t) = r_1(t)\cos(\omega t) + s_1(t)\sin(\omega t)\,, \tag{40}$$

where the vectors $r_1(t), s_1(t) \in \mathbb{R}^2$ are T-periodic and may contain terms such as $\sin(k\omega t)$ and $\cos(k\omega t)$ for $k = 1, \ldots, \infty$.

Substituting (32) and (40) into (22), and collecting terms according to $\sin(\omega t)$ and $\cos(\omega t)$, we obtain

$$\begin{aligned} \dot{\chi}_1 &= \overline{A}_1(\xi_1)\chi_1 + \overline{B}_1 u\,, \\ \tilde{v}_{1s}(t) &= \big[\cos(\omega t)\ \sin(\omega t)\big]\,\overline{C}_1\chi_1 \\ &= C_1 r_1(t)\cos(\omega t) + C_1 s_1(t)\sin(\omega t) \\ &= \Lambda_1(t)\sin\big(\omega t + \theta_1(t)\big)\,, \end{aligned} \tag{41}$$

where

$$\begin{aligned} &\chi_1 = \begin{bmatrix} r_1 \\ s_1 \end{bmatrix}, \quad u = \begin{bmatrix} r_0 \\ s_0 \end{bmatrix}, \quad \overline{A}_1(\xi_1) = \begin{bmatrix} A_1(\xi_1) & -\omega I_2 \\ \omega I_2 & A_1(\xi_1) \end{bmatrix}, \\ &\overline{B}_1 = I_2 \otimes B_1\,, \quad \overline{C}_1 = I_2 \otimes C_1\,, \quad \theta_1 = \arctan\left(\frac{C_1 r_1}{C_1 s_1}\right), \\ &\Lambda_1 = \sqrt{\big(C_1 r_1\big)^2 + \big(C_1 s_1\big)^2} = \sqrt{(\overline{C}_1\chi_1)^{\mathrm{T}}(\overline{C}_1\chi_1)}\,, \end{aligned} \tag{42}$$

where $A_1(\xi_1), B_1, C_1$ are given by (23). The quantity $\Lambda_1(t)$ gives an upper bound for $v_{1\mathrm{s}}$ since $\|\tilde{v}_{1\mathrm{s}}\|_\infty \le \|\Lambda_1\|_\infty$ based on the second equation in (41). We assume that $\Lambda_1(t)$ is a continuous and smooth function of time t such that its supremum occurs when

$$\dot{\Lambda}_1(t) = \frac{(\overline{C}_1\chi_1)^{\mathrm{T}}(\overline{C}_1\dot{\chi}_1)}{2\sqrt{(\overline{C}_1\chi_1)^{\mathrm{T}}(\overline{C}_1\chi_1)}} = 0\,. \tag{43}$$

There are three possible solutions for (43) that are $\dot{\chi} = 0$, $\overline{C}_1\chi_1 \perp \overline{C}_1\dot{\chi}_1$, and $\overline{C}_1 \perp \dot{\chi}_1$. However, for the weak nonlinearities $|V^{(n)}(h)| \le \frac{\pi^n}{2\times 30^{n-1}}$ (cf. (2) and (3)), we find that the supremum always occurs at $\dot{\chi}_1 = 0$. Substituting this into the first equation of (41) yields $\chi_1 = -(\overline{A}_1(\xi_1))^{-1}\overline{B}_1 u$. Plugging this into (42) leads to

$$\|\Lambda_1\|_\infty = \sqrt{\big(\overline{C}_1(\overline{A}_1(\xi_1))^{-1}\overline{B}_1 u\big)^{\mathrm{T}}\big(\overline{C}_1(\overline{A}_1(\xi_1))^{-1}\overline{B}_1 u\big)}\,. \tag{44}$$

The right hand side of (44) is continuous in terms of elements in $\overline{A}_1(\xi_1)$, which are bounded for $\forall \xi_1 \in \mathscr{D}$; cf. (12), (14), (23) and (42). Thus, there exists a constant $\xi_1^* \in \mathscr{D}$ where $\|\Lambda_1\|_\infty$ reaches its maximum such that

$$\begin{aligned} \|\Lambda_1\|_\infty &\le \sqrt{\big(\overline{C}_1(\overline{A}_1(\xi_1^*))^{-1}\overline{B}_1 u\big)^{\mathrm{T}}\big(\overline{C}_1(\overline{A}_1(\xi_1^*))^{-1}\overline{B}_1 u\big)} \\ &= \sqrt{\Gamma_{1,0}(\omega)}\sqrt{r_0^2 + s_0^2} = \sqrt{\Gamma_{1,0}(\omega)}\|\tilde{v}_0\|_\infty\,, \end{aligned} \tag{45}$$

where the amplification ratio is given by

$$\Gamma_{1,0}(\omega) = \frac{\omega^2\beta_1^2 + \varphi_1(\xi_1^*)^2}{\omega^4 + (\kappa_1^2 - 2\varphi_1(\xi_1^*))\omega^2 + \varphi_1^2(\xi_1^*)}\,. \tag{46}$$

Since $\|\tilde{v}_{1\mathrm{s}}\|_\infty \le \|\Lambda\|_\infty \le \sqrt{\Gamma_{1,0}}\|\tilde{v}_0\|_\infty$, the head-to-tail string stability (19) of motif 1 is ensured if $\Gamma_{1,0}(\omega) < 1$ for $\forall \omega \in \mathbb{R}_+$. This is equivalent to that the difference between the denominator and the numerator of (46) is always positive. That yields

$$\omega^2\Big(\omega^2 + \alpha_1\big(\alpha_1 + 2\beta_1 - 2V'(\xi_1^*)\big)\Big) > 0\,, \quad \forall \omega \in \mathbb{R}_+\,. \tag{47}$$

To guarantee that this inequality holds for $\forall \alpha_1 > 0$, one needs

$$\alpha_1 + 2\beta_1 - 2V'(\xi_1^*) > 0\,, \tag{48}$$

which implies that larger α_1 or β_1 are required when $V'(\xi_1^*)$ increases. In this sense, the worst-case scenario occurs when

$$\xi_1^* = 20\ [\mathrm{m}]\,, \quad V'(\xi_1^*) = \max_{\forall \xi_1 \in \mathscr{D}} V'(\xi_1) = \pi/2\ [1/\mathrm{s}]\,, \tag{49}$$

cf. (2) and (12). Substituting (49) into (48) leads to

$$\alpha_1 + 2\beta_1 - \pi > 0\,, \tag{50}$$

which is a sufficient condition for the head-to-tail string stability of motif 1 network. We remark that this condition is equivalent to the string stability condition derived in [3] for the linearized system in the most conservative case.

4 STABILITY ANALYSIS OF MOTIF 2

In case of motif 2, the CCC vehicle reacts to the motion of the nearest two vehicles in front; see Fig. 2(c). The car-following dynamics of motif 2 is governed by

$$\begin{aligned}
\dot{h}_1 &= v_0 - v_1\,,\\
\dot{v}_1 &= \alpha_1\big(V(h_1) - v_1\big) + \beta_1(v_0 - v_1)\,,\\
\dot{h}_2 &= v_1 - v_2\,,\\
\dot{v}_2 &= \alpha_1\big(V(h_2) - v_2\big) + \beta_1(v_1 - v_2)\\
&\quad + \alpha_2\Big(V\Big(\frac{h_1+h_2}{2}\Big) - v_2\Big) + \beta_1(v_0 - v_2)\,,
\end{aligned} \tag{51}$$

cf. (5). Following (7)–(15), one can obtain the perturbation model of motif 2 in the form

$$\begin{aligned}
\dot{X}_2 &= A_2(\Xi_2)X_2 + B_2\tilde{v}_0\,,\\
\tilde{v}_2 &= C_2X_2\,,
\end{aligned} \tag{52}$$

where $\Xi_2 = [\xi_1, \xi_2, \eta_2]^{\mathrm{T}} \in \mathscr{D}^3$ and

$$\begin{aligned}
A_2(\Xi_2) &= \begin{bmatrix} A_1(\xi_1) & 0_{2\times 2} \\ A_{2,1}(\eta_2) & A_{2,2}(\xi_2,\eta_2) \end{bmatrix}, \quad B_2 = \begin{bmatrix} B_1 \\ B_{2,2} \end{bmatrix},\\
C_2 &= \begin{bmatrix} 0_{1\times 2} & C_{2,2} \end{bmatrix}.
\end{aligned} \tag{53}$$

Here $A_1(\xi_1), B_1$ are given by (23) while other matrices are

$$\begin{aligned}
A_{2,1}(\eta_2) &= \begin{bmatrix} 0 & 1 \\ \varphi_2(\eta_2) & \beta_1 \end{bmatrix}, \quad B_{2,2} = \begin{bmatrix} 0 \\ \beta_2 \end{bmatrix}, \quad C_{2,2} = \begin{bmatrix} 0 & 1 \end{bmatrix},\\
A_{2,2}(\xi_2,\eta_2) &= \begin{bmatrix} 0 & -1 \\ \varphi_1(\xi_2) + \varphi_2(\eta_2) & -\kappa_1 - \kappa_2 \end{bmatrix}.
\end{aligned} \tag{54}$$

4.1 Plant Stability of Motif 2

Since motif 2 is plant unstable if vehicle 1 loses plant stability, we assume that the plant stability of vehicle 1 has been ensured by (31). Thus, we only need to investigate the plant stability of the CCC vehicle 2. Its motion is governed by

$$\begin{aligned}
\dot{x}_2 &= A_{2,2}(\xi_2,\eta_2)x_2 + A_{2,1}(\xi_2)x_1 + B_{2,2}\tilde{v}_0\,,\\
\tilde{v}_2 &= C_{2,2}x_2\,,
\end{aligned} \tag{55}$$

which can be obtained from (52) while matrices $A_{2,1}(\xi_2)$, $A_{2,2}(\xi_2,\eta_2)$, $B_{2,2}$ and $C_{2,2}$ are given by (54).

When studying the plant stability of vehicle 2, we neglect the excitation arising from vehicle 0 and vehicle 1, i.e., $\tilde{v}_0(t) \equiv 0$ and $x_1(t) \equiv 0$. Then, the plant stability of vehicle 2 can be ensured by finding a Lyapunov function $L = x_2^{\mathrm{T}}Px_2 > 0$ such that

$$\dot{L} = x_2^{\mathrm{T}}\big((A_{2,2}(\xi_2,\eta_2))^{\mathrm{T}}P + PA_{2,2}(\xi_2,\eta_2)\big)x_2 < 0\,, \tag{56}$$

for $\forall \xi_2, \eta_2 \in \mathscr{D}$. Since $A_{2,2}(\xi_2,\eta_2)$ in (54) is analogous to $A_1(\xi_1)$ given by (23), the plant stability conditions for vehicle 2 can be obtained using (27) and (28) while replacing $\varphi_1(\xi_1)$ by $\varphi_1(\xi_2) + \varphi_2(\eta_2)$, and κ_1 by $\kappa_1 + \kappa_2$. Then, using (14), we obtain

$$\begin{aligned}
\alpha_1 + \beta_1 + \alpha_2 + \beta_2 + \frac{p_2}{p_3} &> 0\,,\\
\left(\frac{\pi p_3}{8p_2} + 1\right)\alpha_1 + \beta_1 + \left(\frac{\pi p_3}{16p_2} + 1\right)\alpha_2 + \beta_2 + \frac{p_2}{p_3} &> 0\,.
\end{aligned} \tag{57}$$

4.2 String Stability of Motif 2

Here, we show that the head-to-tail string stability can be ensured by designing the dynamics of the CCC vehicle 2, even when vehicle 1 is string unstable. Following the analysis for motif 1, it can be shown that, if the condition (57) holds, the sinusoidal perturbation $\tilde{v}_0(t)$ in (32) leads to periodic steady-state perturbations for the following vehicles with period $T = 2\pi/\omega$. That is,

$$\begin{aligned}
x_{j\mathrm{s}}(t) &= \sum_{k=1}^{\infty} r_{j,k}\cos(k\omega t) + s_{j,k}\sin(k\omega t)\\
&= r_j(t)\cos(\omega t) + s_j(t)\sin(\omega t)\,, \quad j = 1,2\,,
\end{aligned} \tag{58}$$

where $r_{j,k}, s_{j,k} \in \mathbb{R}^2$ are constant vectors while the vectors $r_j(t), s_j(t) \in \mathbb{R}^2$ are T-periodic and may contain terms like $\sin(k\omega t)$ and $\cos(k\omega t)$ for $k = 1,\ldots,\infty$; cf. (39), (40). When analyzing the head-to-tail string stability of motif 2, we use the model (52). Substituting (32) and (58) into (52) and collecting terms according to $\sin(\omega t)$ and $\cos(\omega t)$ leads to

$$\begin{aligned}
\dot{\chi}_2 &= \overline{A}_2(\Xi_2)\chi_2 + \overline{B}_2u\,,\\
\tilde{v}_{2\mathrm{s}}(t) &= \begin{bmatrix}\cos(\omega t) & \sin(\omega t)\end{bmatrix}\overline{C}_2\chi_2\\
&= C_2R_2(t)\cos(\omega t) + C_2S_2(t)\sin(\omega t)\\
&= \Lambda_2(t)\sin\big(\omega t + \theta_2(t)\big)\,,
\end{aligned} \tag{59}$$

where

$$\chi_2 = \begin{bmatrix} R_2 \\ S_2 \end{bmatrix}, \quad R_2 = \begin{bmatrix} r_1 \\ r_2 \end{bmatrix}, \quad S_2 = \begin{bmatrix} s_1 \\ s_2 \end{bmatrix},$$
$$\overline{A}_2(\Xi_2) = \begin{bmatrix} A_2(\Xi_2) & -\omega I_4 \\ \omega I_4 & A_2(\Xi_2) \end{bmatrix}, \quad \overline{B}_2 = I_2 \otimes B_2, \quad \overline{C}_2 = I_2 \otimes C_2,$$
$$\Lambda_2 = \sqrt{\big(C_2 R_2\big)^2 + \big(C_2 S_2\big)^2} = \sqrt{(\overline{C}_2\chi_2)^{\mathrm{T}}(\overline{C}_2\chi_2)},$$
$$\theta_2 = \arctan\left(\frac{C_2 R_2}{C_2 S_2}\right), \tag{60}$$

where $A_2(\Xi_2)$, B_2, C_2 are given by (53). From the second equation of (59), we have $\|\tilde{v}_{2s}\|_\infty \le \|\Lambda_2\|_\infty$. Due to the weak nonlinearities, we again postulate that the supremum of Λ_2 occurs at $\dot{\chi}_2 = 0$, leading to $\chi_2 = (\overline{A}_2(\Xi_2))^{-1}\overline{B}_2 u$. Substituting this in (60) results in

$$\|\Lambda_2\|_\infty = \sqrt{\big(\overline{C}_2(\overline{A}_2(\Xi_2))^{-1}\overline{B}_2 u\big)^{\mathrm{T}}\big(\overline{C}_2(\overline{A}_2(\Xi_2))^{-1}\overline{B}_2 u\big)}. \tag{61}$$

Since $\|\Lambda_2\|_\infty$ is continuous in terms of the elements in $\overline{A}_2(\Xi_2)$, which are bounded for $\forall \Xi_2 \in \mathscr{D}^3$, there exist constants $\Xi_2^* \in \mathscr{D}^3$ where $\|\Lambda_2\|_\infty$ reaches its maximum, that is,

$$\begin{aligned} \|\Lambda_2\|_\infty &\le \sqrt{\big(\overline{C}_2(\overline{A}_2(\Xi_2^*))^{-1}\overline{B}_2 u\big)^{\mathrm{T}}\big(\overline{C}_2(\overline{A}_2(\Xi_2^*))^{-1}\overline{B}_2 u\big)} \\ &= \sqrt{\Gamma_{2,0}(\omega)(r_0^2 + s_0^2)} = \sqrt{\Gamma_{2,0}(\omega)}\|\tilde{v}_0\|_\infty. \end{aligned} \tag{62}$$

Here the amplification ratio is

$$\Gamma_{2,0}(\omega) = \frac{n_3\omega^6 + n_2\omega^4 + n_1\omega^2 + n_0}{\omega^8 + d_3\omega^6 + d_2\omega^4 + d_1\omega^2 + d_0}, \tag{63}$$

where

$$\begin{aligned} n_3 &= \beta_2^2, \\ n_2 &= 2\beta_1^2\beta_2\kappa_1 + \beta_2^2\kappa_1^2 - 2\beta_1\beta_2\big(\varphi_1(\xi_1^*) + \varphi_1(\xi_2^*)\big) \\ &\quad - 2\beta_2^2\varphi_1(\xi_1^*) + \beta_1^4 + \varphi_2^2(\eta_2^*) + 2\beta_1^2\varphi_2(\eta_2^*), \\ n_1 &= \beta_1^2\varphi_1^2(\xi_2^*) + (\beta_1^2 + \beta_2^2 + 2\beta_1\beta_2)\varphi_1^2(\xi_1^*) \\ &\quad + 2\big(\beta_1\kappa_1 - 2\varphi_2(\eta_2^*) - \beta_1^2\big)\varphi_2(\eta_2^*)\varphi_1(\xi_1^*) + 2\beta_1\kappa_1\varphi_1(\xi_2)\varphi_2(\eta_2^*) \\ &\quad + 2\big(\beta_1\beta_2 - \beta_2\kappa_1 - \varphi_2(\eta_2^*)\big)\varphi_1(\xi_1^*)\varphi_1(\xi_2^*) + \kappa_1^2\varphi_2^2(\eta_2^*), \\ n_0 &= \varphi_1^2(\xi_1^*)\varphi_1^2(\xi_2^*) + \varphi_1^2(\xi_1^*)\varphi_2^2(\eta_2^*) + 2\varphi_1^2(\xi_1^*)\varphi_1(\xi_2^*)\varphi_2(\eta_2^*), \\ d_3 &= -2\varphi_2(\eta_2^*) - 2\varphi_1(\xi_1^*) - 2\varphi_1(\xi_2^*) + \kappa_2^2 + 2\kappa_1^2 + 2\kappa_1\kappa_2, \\ d_2 &= \varphi_2^2(\eta_2^*) + 2\big(2\varphi_1(\xi_1^*) + \varphi_1(\xi_2^*) - \kappa_1^2\big)\varphi_2(\eta_2^*) + \varphi_1^2(\xi_2^*) \\ &\quad + 2\big(2\varphi_1(\xi_1^*) - \kappa_1^2\big)\varphi_1(\xi_2^*) + \varphi_1^2(\xi_1^*) + \kappa_1^4 + 2\kappa_1^3\kappa_2 \\ &\quad - 2\big(\kappa_1^2 + \kappa_2^2 + 2\kappa_1\kappa_2\big)\varphi_1(\xi_1^*), \\ d_1 &= (\kappa_1^2 - 2\varphi_1(\xi_1^*))\varphi_2^2(\eta^*) + \big(\kappa_1^2 - 2\varphi_1(\xi_1^*)\big)\varphi_1^2(\xi_2^*) \\ &\quad + 2\big(\big(\kappa_1^2 - 2\varphi_1(\xi_1^*)\big)\varphi_1(\xi_2^*) - 2\varphi_1^2(\xi_1^*)\big)\big)\varphi_2(\eta_2^*) \\ &\quad - 2\varphi_1^2(\xi_1^*)\varphi_1(\xi_2^*) + (\kappa_1^2 + \kappa_2^2)^2\varphi_1^2(\xi_1^*), \\ d_0 &= n_0. \end{aligned} \tag{64}$$

Since $\|\tilde{v}_{2s}\|_\infty \le \|\Lambda_2\|_\infty \le \sqrt{\Gamma_{2,0}}\|\tilde{v}_0\|_\infty$, motif 2 is head-to-tail string stable if $\Gamma_{2,0}(\omega) < 1$ for $\forall\omega \in \mathbb{R}_+$. This holds if the difference between the denominator and the numerator of (63) is positive such that

$$\omega^2\big(\omega^6 + (d_3 - n_3)\omega^4 + (d_2 - n_2)\omega^2 + (d_1 - n_1)\big) > 0, \tag{65}$$

for $\forall\omega \in \mathbb{R}_+$. To satisfy (65), it is necessary that

$$\begin{aligned} d_1 - n_1 &= 2\alpha_1^2\beta_2 V'(\xi_1^*)(\alpha_1 V'(\xi_1^*) + \alpha_1 V'(\xi_2^*) + \alpha_2 V'(\xi_1^*)) \\ &\quad + \alpha_1^2\alpha_2^2\big(V'(\xi_1^*)\big)^2 + a_1\alpha_1^2\alpha_2 + a_0\alpha_1^2 > 0, \end{aligned} \tag{66}$$

where

$$\begin{aligned} a_0 &= V'(\xi_1^*)\big(\alpha_1 + 2\beta_1 - 2V'(\xi_2^*)\big) + V'(\xi_2^*)\big(\alpha_1 + 2\beta_1 - 2V'(\xi_1^*)\big), \\ a_1 &= V'(\eta_2^*)\big(\alpha_1 V'(\xi_2^*) - V'(\xi_1^*)V'(\xi_2^*) - \beta_1 V'(\xi_1^*) + \beta_1 V'(\xi_2^*)\big) \\ &\quad + \big(V'(\xi_1^*)\big)^2\big(2\alpha_1 + 2\beta_1 - V'(\eta_2^*)\big). \end{aligned} \tag{67}$$

When $a_0 < 0$ and $a_1 < 0$ decreases, larger α_2 or β_2 are required to satisfy (66), leading to small head-to-tail string stable domain. Thus, the smallest a_0 and a_1 correspond to the worst-case scenario. Note that ξ_1^* is related to vehicle 1 while ξ_2^*, η_2^* are related to vehicle 2. We consider that vehicle 1 is string unstable such that $\alpha_1 + 2\beta_1 - 2V'(\xi_1^*) < 0$ and in the worst-case scenario (49). Then, to find the minimum of a_0, we solve

$$\frac{\partial a_0}{\partial \xi_2^*} = \frac{\pi^2 v_{\max}\big(\alpha_1 + 2\beta_1 - 4V'(\xi_1^*)\big)}{2(h_{\mathrm{go}} - h_{\mathrm{st}})^2}\cos\left(\pi\frac{\xi_2^* - h_{\mathrm{st}}}{h_{\mathrm{go}} - h_{\mathrm{st}}}\right) = 0, \tag{68}$$

for ξ_2^*. Note that $\alpha_1 + 2\beta_1 - 4V'(\xi_1^*) < \alpha_1 + 2\beta_1 - 2V'(\xi_1^*) < 0$. Thus, the solution of (68) is

$$\xi_2^* = (h_{\mathrm{go}} + h_{\mathrm{st}})/2 = 20\ [\mathrm{m}], \quad V'(\xi_2^*) = \pi/2\ [1/\mathrm{s}]. \tag{69}$$

Plugging (49) and (69) into the second equation of (67), and solving $\partial a_1/\partial \eta_2^* = 0$, we can also show that the minimum of a_1 occurs at

$$\eta_2^* = (h_{\rm go} + h_{\rm st})/2 = 20\ [\rm m]\,, \quad V'(\eta_2^*) = \pi/2\ [1/\rm s]\,. \tag{70}$$

Substituting (49), (69) and (70) into (64) and (65) leads to head-to-tail string stability conditions, but solutions cannot be obtained analytically. Thus, we utilize the D-subdivision method [11] and seek the stability boundaries. Dividing (65) by ω^2 and collecting terms according to α_2 and β_2 yields

$$\Theta(\omega) = U_1 + U_2(\alpha_2^2 + 2\alpha_2\beta_2) + U_3\alpha_2 + U_4\beta_2 > 0\,, \tag{71}$$

for $\forall \omega > 0$, where

$$\begin{aligned}
U_1 &= \omega^6 + 2(2\alpha_1\beta_1 - \alpha_1\pi + \alpha_1^2 + \beta_1^2)\omega^4 + \Big[\frac{3}{2}\alpha_1^2\pi^2 + 6\alpha_1^2\beta_1^2 \\
&\quad - 2\alpha_1(2\alpha_1\beta_1 + \alpha_1^2 + \beta_1^2)\pi + \alpha_1(4\beta_1^3 + 4\alpha_1^2\beta_1 + \alpha_1^3)\Big]\omega^2 \\
&\quad + \frac{\alpha_1^2\pi^2}{4}(2\beta_1 - \pi + 3\alpha_1)\,, \\
U_2 &= \omega^4 + (\alpha_1^2 + \beta_1^2 - \alpha_1\pi + 2\alpha_1\beta_1)\omega^2 + \frac{1}{4}\alpha_1^2\pi^2\,, \\
U_3 &= \Big(2\alpha_1 + 2\beta_1 - \frac{\pi}{2}\Big)\omega^4 + \Big[\frac{3}{4}\alpha_1\pi^2 - \Big(3\alpha_1\beta_1 + \beta_1^2 - \frac{5}{2}\alpha_1^2\Big)\pi \\
&\quad + 2(\alpha_1^3 + \beta_1^3 + 3\alpha_1^2\beta_1 + 3\alpha_1\beta_1^2)\Big]\omega^2 + \frac{\alpha_1^2\pi^2}{4}(2\beta_1 - \pi + 3\alpha_1)\,, \\
U_4 &= 2(\alpha_1 + \beta_1)\omega^4 + 2\alpha_1(2\beta_1^2 + \alpha_1^2 + 3\alpha_1\beta_1 - \alpha_1\pi)\omega^2 + \alpha_1^3\pi^2\,.
\end{aligned} \tag{72}$$

At the boundary, we have $\Theta(\omega) = 0$ and $\partial\Theta(\omega)/\partial\omega = 0$, which yields

$$\begin{aligned}
\alpha_2(\omega) &= \frac{-2U_2W_1 - U_3 - U_4W_2 \pm \sqrt{\Delta}}{2(U_2 + 2W_2)}\,, \\
\beta_2(\omega) &= W_1 + W_2\alpha_2(\omega)\,,
\end{aligned} \tag{73}$$

where

$$\begin{aligned}
W_1 &= \frac{(\partial_\omega U_1)U_2 - U_1(\partial_\omega U_2)}{(\partial_\omega U_2)U_4 - U_2(\partial_\omega U_4)}\,, \quad W_2 = \frac{(\partial_\omega U_3)U_2 - U_3(\partial_\omega U_2)}{(\partial_\omega U_2)U_4 - U_2(\partial_\omega U_4)}\,, \\
\Delta &= (2U_2W_1 + U_3 + U_4W_2)^2 - 4(U_2 + 2W_2)(U_1 + U_4W_1)\,.
\end{aligned} \tag{74}$$

Here $\partial_\omega U_j$ denotes the differentiation of U_j with respect to ω.

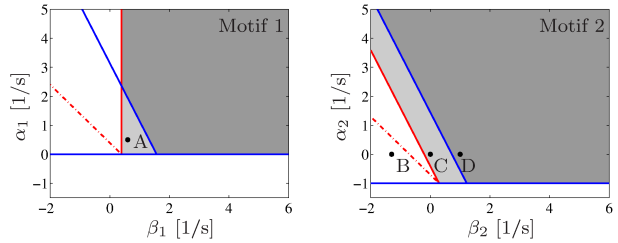

FIGURE 3. Stability diagrams for motif 1 (left) and motif 2 (right). For motif 2, we choose $\alpha_1 = 0.5$ [1/s] and $\beta_1 = 0.6$ [1/s] as shown by point A in left panel. Red lines and blue lines denote the plant stability boundary and the head-to-tail string stability boundary, respectively. The plant stable domain and the head-to-tail string stable domain are shaded by light gray and dark gray, respectively.

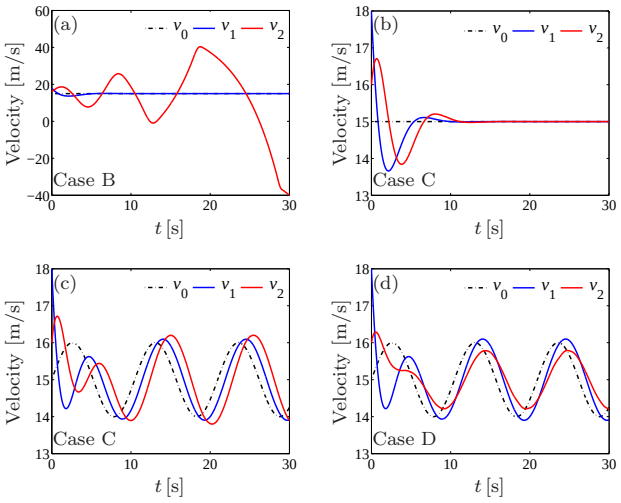

FIGURE 4. Simulation results for motif 2. (a,b): simulations for points B and C in terms of plant stability; (c,d): simulations for points C and D in terms of head-to-tail string stability.

For $\omega \to 0$, applying L'Hôpital's rule in (73) leads to the zero-frequency boundary

$$\alpha_2 = -2\alpha_1\,, \quad \alpha_2 = -2\beta_2 - \alpha_1 - 2\beta_1 + \pi\,. \tag{75}$$

Plotting the boundaries (73) and (75) for all $\omega \geq 0$ in the (β_2, α_2)-plane leads to the head-to-tail string stability diagram for motif 2.

5 STABILITY DIAGRAMS AND SIMULATIONS

Stability diagrams for motifs 1 and 2 are demonstrated by the left and the right panels in Fig. 3, respectively, where the red lines indicate the plant stability boundaries (31) and (57) while the blue lines are the string stability boundaries (50) and (75).

Here, the plant stable and the head-to-tail string stable domains are indicated by light gray and dark gray shadings, respectively. Note that $p_2 = -\pi$ and $p_3 = 8$ are used when plotting the plant stability boundaries, as discussed in Section 3.1. The dash-dotted and the solid red lines denote the plant stability boundaries given by the first and the second inequalities in (31) and (57), respectively. For motif 2, we consider that vehicle 1 is plant stable but string unstable, and then set $(\alpha_1,\ \beta_1) = (0.6,\ 0.7)$ [1/s], as marked by point A in Fig. 3.

To demonstrate the stability behavior of motif 2, we select the points B–D in Fig. 3. Point C ($\alpha_2 = \beta_2 = 0$) implies that there is no communication between vehicle 0 and vehicle 2. We set the initial conditions $h_1(0) = 18$ [m], $v_1(0) = 18$ [m/s], $h_2(0) = 22$ [m], and $v_2(0) = 16$ [m/s]. To show the plant stability of motif 2, we assume that vehicle 0 moves at the constant speed $v_0(t) \equiv 15$ [m/s]. The simulation results corresponding to cases B and C are shown in Fig. 4(a) and (b), which show that case B is plant unstable while case C is plant stable. To demonstrate the head-to-tail string stability of motif 2, we assume the speed of vehicle 0 as $v_0(t) = 15 + \sin(0.6t)$ [m/s], where the sinusoidal term can be seen as a perturbation to the head vehicle. The simulation results corresponding to cases C and D are demonstrated in Fig. 4(c) and (d). When there is no communication between vehicle 0 and vehicle 2 (case C), the disturbance is amplified when propagating upstream. But if vehicle 2 utilizes the information received from vehicle 0 (case D), the disturbance is attenuated by vehicle 2 even though vehicle 1 amplifies the signal. This demonstrates the advantages of V2V communication in stabilizing a platoon.

It should be pointed out that the stable domain for motif 2 (the right panel in Fig. 3) covers the negative control gains, implying that one may stabilize motif 2 network by using negative gains α_2 and/or β_2.

6 CONCLUSIONS

In this paper, we investigated the nonlinear dynamics of connected vehicle systems and analyzed their plant stability and head-to-tail string stability. The results were summarized using stability diagrams, which allows one to select control gains in order to ensure stability of vehicle networks. In practice, vehicle-to-vehicle communication may lead to delays for receiving information due to intermittency and packet drops. Also, the communication may be lost due to sensor faults or signal disconnection, resulting in variation of connectivity structures. The robustness of the connected vehicle systems against communication delays and variation of connectivity structures will be studied in future. We remark that the plant stability and the string stability are related to safety of vehicles but do not necessarily guarantee collision-free behavior. Ensuring stability and safety simultaneously is another future research direction.

REFERENCES

[1] Naus, G. J. L., Vugts, R. P. A., Ploeg, J., van de Molengraft, M. J. G., and Steinbuch, M., 2010. "String-stable CACC design and experimental validation: A frequency-domain approach". *IEEE Transactions on Vehicular Technology,* **59**(9), pp. 4268–4279.

[2] Kianfar, R., Augusto, B., Ebadighajari, A., Hakeem, U., Nilsson, J., Raza, A., Tabar, R. S., Irukulapati, N. V., Englund, C., Falcone, P., Papanastasiou, S., Svensson, L., and Wymeersch, H., 2012. "Design and experimental validation of a cooperative driving system in the grand cooperative driving challenge". *IEEE Transactions on Intelligent Transportation Systems,* **13**(3), pp. 994–1007.

[3] Zhang, L., and Orosz, G., 2013. "Designing network motifs in connected vehicle systems: delay effects and stability". In Proceedings of the ASME Dynamic Systems and Control Conference, no. DSCC2013-4081, p. V003T42A006.

[4] Ge, J. I., and Orosz, G., 2014. "Dynamics of connected vehicle systems with delayed acceleration feedback". *Transportation Research Part C,* **46**, pp. 46–64.

[5] Qin, W. B., Gomez, M. M., and Orosz, G., 2014. "Stability analysis of connected cruise control with stochastic delays". In American Control Conference, pp. 5534–5539.

[6] Orosz, G., 2014. "Connected cruise control: modeling, delay effects, and nonlinear behavior". *Vehicle System Dynamics,*(submitted).

[7] Zhang, L., and Orosz, G., 2014. "Motif-based analysis of connected vehicle systems: delay effects and stability". *Automatica*, p. (submitted).

[8] Orosz, G., Wilson, R. E., and Stépán, G., 2010. "Traffic jams: dynamics and control". *Philosophical Transactions of the Royal Society A,* **368**(1928), pp. 4455–4479.

[9] Orosz, G., and Shah, S. P., 2012. "A nonlinear modeling framework for autonomous cruise control". In Proceedings of the ASME Dynamic Systems and Control Conference.

[10] Khalil, H. K., 2002. *Nonlinear Systems (3rd Edition)*. Prentice Hall, New Jersey.

[11] Insperger, T., and Stépán, G., 2011. *Semi-discretization for time-delay systems*. Springer, New York.